

The Necklace: equatorial and polar outflows from the binary central star of the new planetary nebula IPHASX J194359.5+170901

R. L. M. Corradi,^{1,2*} L. Sabin,³ B. Miszalski,⁴ P. Rodríguez-Gil,^{1,2,5}
M. Santander-García,^{1,2,5} D. Jones,⁶ J. E. Drew,⁴ A. Mampaso,^{1,2} M. J. Barlow,⁷
M. M. Rubio-Díez,^{5,8} J. Casares,^{1,2} K. Viironen,^{9,10} D. J. Frew,¹¹ C. Giammanco,^{1,2}
R. Greimel¹² and S. E. Sale^{13,14}

¹*Instituto de Astrofísica de Canarias, E-38200 La Laguna, Tenerife, Spain*

²*Departamento de Astrofísica, Universidad de La Laguna, E-38206 La Laguna, Tenerife, Spain*

³*Instituto de Astronomía, Universidad Nacional Autónoma de México, Apdo. Postal 877, 22800 Ensenada, B.C., Mexico*

⁴*Centre for Astrophysics Research, STRI, University of Hertfordshire, College Lane Campus, Hatfield AL10 9AB*

⁵*Isaac Newton Group of Telescopes, Apart. de Correos 321, 38700 Santa Cruz de la Palma, Spain*

⁶*Jodrell Bank Centre for Astrophysics, School of Physics and Astronomy, University of Manchester, Manchester M13 9PL*

⁷*Department of Physics and Astronomy, University College London, Gower Street, London WC1E 6BT*

⁸*Centro de Astrobiología, CSIC-INTA, Ctra de Torrejón a Ajalvir km 4, E-28850 Torrejón de Ardoz, Spain*

⁹*Centro Astronómico Hispano Alemán, Calar Alto, C/Jesús Durbán Remón 2-2, E-04004 Almería, Spain*

¹⁰*Centro de Estudios de Física del Cosmos de Aragón (CEFCA), C/General Pizarro 1-1, E-44001 Teruel, Spain*

¹¹*Department of Physics and Astronomy, Macquarie University, North Ryde, NSW 2109, Australia*

¹²*Institut für Physik, Karl-Franzen Universität Graz, Universitätsplatz 5, 8010 Graz, Austria*

¹³*Dept. de Física y Astronomía, Universidad de Valparaíso, Ave. Gran Bretaña 1111, Playa Ancha, Casilla 53, Valparaíso, Chile*

¹⁴*Dept. de Astronomía y Astrofísica, Pontificia Universidad Católica de Chile, Av. Vicuña Mackenna 4860, Casilla 306, Santiago 22, Chile*

Accepted 2010 August 13. Received 2010 August 12; in original form 2010 June 21

ABSTRACT

IPHASX J194359.5+170901 is a new high-excitation planetary nebula with remarkable characteristics. It consists of a knotty ring expanding at a speed of 28 km s^{-1} , and a fast collimated outflow in the form of faint lobes and caps along the direction perpendicular to the ring. The expansion speed of the polar caps is $\sim 100 \text{ km s}^{-1}$, and their kinematical age is twice as large as the age of the ring.

Time-resolved photometry of the central star of IPHASX J194359.5+170901 reveals a sinusoidal modulation with a period of 1.16 d. This is interpreted as evidence for binarity of the central star, the brightness variations being related to the orbital motion of an irradiated companion. This is supported by the spectrum of the central star in the visible range, which appears to be dominated by emission from the irradiated zone, consisting of a warm (6000–7000 K) continuum, narrow C III, C IV and N III emission lines, and broader lines from a flat H I Balmer sequence in emission.

IPHASX J194359.5+170901 helps to clarify the role of (close) binaries in the formation and shaping of planetary nebulae (PNe). The output of the common-envelope (CE) evolution of the system is a strongly flattened circumstellar mass deposition, a feature that seems to be distinctive of this kind of binary system. Also, IPHASX J194359.5+170901 is among the first post-CE PNe for which the existence of a high-velocity polar outflow has been demonstrated. Its kinematical age might indicate that the polar outflow is formed before the CE phase. This points to mass transfer on to the secondary as the origin, but alternative explanations are also considered.

Key words: binaries: close – stars: winds, outflows – ISM: abundances – ISM: jets and outflows – planetary nebulae: individual: IPHASX J194359.5+170901.

1 INTRODUCTION

The IPHAS H α survey of the Northern Galactic plane (Drew et al. 2005) provides a wealth of new information about emission-line

*E-mail: rcorradi@iac.es

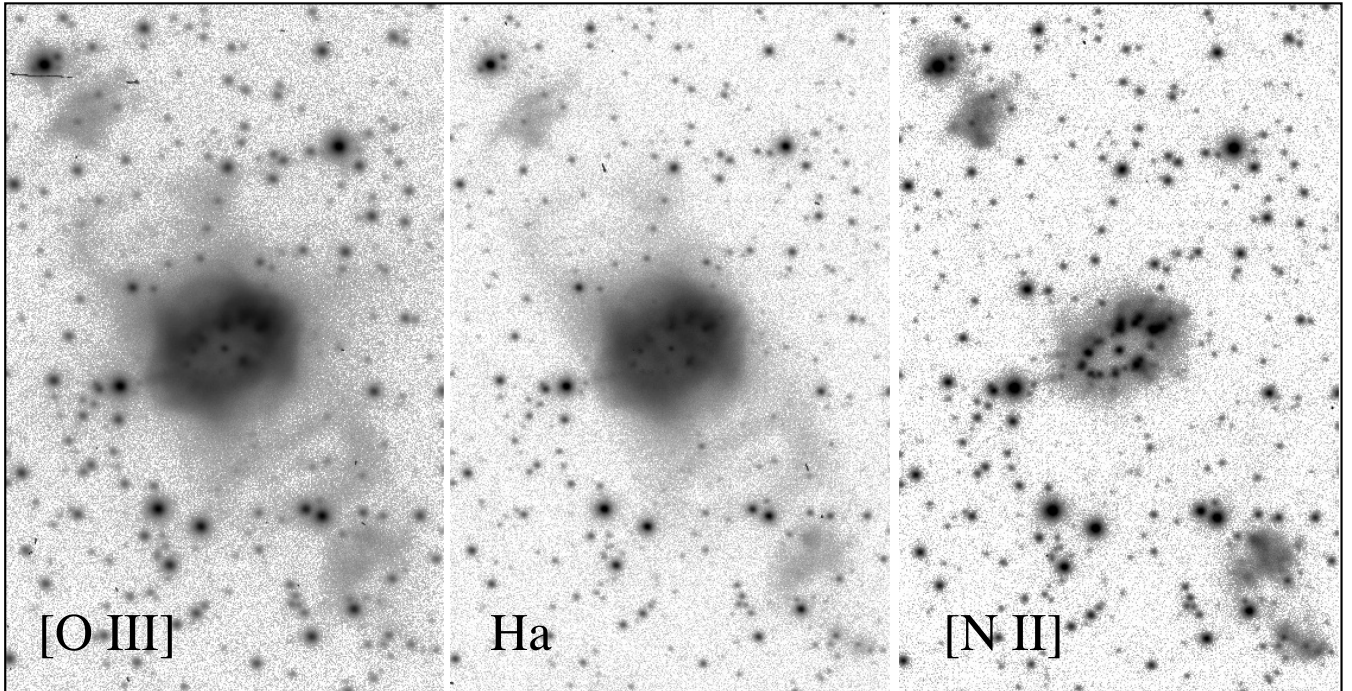


Figure 1. The NOT images of IPHASX J194359.5+170901 in a log intensity scale. The field of view is $70 \times 110 \text{ arcsec}^2$ in each frame. North is up and east is left.

sources. Among them, a large number of planetary nebulae (PNe) are being discovered (Viironen et al. 2009; Sabin et al. 2010, in preparation). Two main objectives can be generally pursued using the IPHAS data on PNe. The first is to determine the global properties of PNe, such as their population size in the Galactic plane and related issues (stellar death rate, global yields, relative contribution of the different morphological classes and their distribution in the disc, etc.). The second objective is to find and study new objects belonging to rare morphological or chemical subclasses, or that have other outstanding characteristics. IPHASX J194359.5+170901 is one of these distinctive new PNe. It is among the brightest new IPHAS PNe in the list of Sabin et al. 2010, in preparation, and its characteristic morphology made it a prime candidate in our ongoing programme looking for binary central stars based on the emerging morphological trends identified with nebulae around close binaries (Miszalski et al. 2009b). In the following, we present imaging, spectroscopy and time-resolved photometry which allow us to determine geometrical, kinematical, physical and chemical properties of the nebula, and to reveal the existence of a close binary central star. This provides a new clarifying example of the relevance of interactions in close binaries for the shaping of PNe – an important and long-standing problem in the field (see De Marco 2009).

2 OBSERVATIONS

IPHASX J194359.5+170901 was discovered as a new candidate PN from images of the IPHAS survey obtained in 2005 (Sabin et al. 2010, in preparation). Deeper and higher resolution images were secured at the 2.6-m Nordic Optical Telescope (NOT) and the ALFOSC spectro-imager on la Palma on 2007 September 3. The filter central wavelengths and full width at half-maximum (FWHM), and the corresponding selected nebular emission lines, were $6589/9 \text{ \AA}$ ([N II] 6583), $6568/8 \text{ \AA}$ ($H\alpha$ 6563) and $5007/30 \text{ \AA}$ ([O III] 5007). Note that the red filters are narrow enough that no

contamination of the [N II] lines occurs in the $H\alpha$ filter and vice versa. In each filter, the exposure time was 20 min. The spatial scale of the ALFOSC instrument is $0.19 \text{ arcsec pixel}^{-1}$, and seeing was 0.6 arcsec FWHM for the $H\alpha$ and [N II] images, and 0.8 arcsec for [O III]. The NOT images are shown in Fig. 1.

With the same instrumentation, medium-resolution long-slit spectra centred on $H\alpha$ were obtained on the same night and in the following one. Grism #17 was used, which provides a spectral dispersion of $0.25 \text{ \AA pixel}^{-1}$, a resolution of 0.7 \AA (FWHM) with the adopted slit width of 0.5 arcsec , and a coverage from 6375 to 6745 \AA . The slit was positioned through the central star of the nebula at several position angles (PAs), namely at $PA = 20^\circ, 34^\circ, 55^\circ, 300^\circ, 330^\circ$ and 355° , in order to map the knotty inner ring-like structure (Fig. 2, upper panel). Exposure times were 10 min, except for the spectrum through $PA = +34^\circ$, where it was 1 h.

A lower resolution spectrum of the nebula and its central star was obtained on the 2007 July 17 with the 4.2-m William Herschel Telescope (WHT) telescope and the double-arm ISIS spectrograph. The long slit of ISIS was opened to 1-arcsec width and positioned at $PA = 121^\circ$, roughly along the major axis of the ring, passing through the central star and the brightest knot on its north-west (NW) side (Fig. 2, lower panel). In the blue arm of ISIS, grating R300B was used, providing a dispersion of $0.86 \text{ \AA pixel}^{-1}$, a resolution of 3 \AA and a spectral coverage from 3200 to 5400 \AA . In the red arm, grating R158R gave a dispersion of $1.82 \text{ \AA pixel}^{-1}$, a resolution of 6 \AA and a spectral coverage from 5400 to 10000 \AA . Note however that due to the dichroic used to split the blue and red lights, and to vignetting inside the spectrograph, flux calibration is uncertain in the range from 5300 to 5600 \AA , and above 9200 \AA . Total exposure times were 40 and 60 min in the blue and red arms, respectively. Seeing was 0.8 arcsec . Several spectrophotometric standards from Oke (1990) were observed during the night, while arcs were only obtained during daytime, a fact that limits the precision of the wavelength calibration.

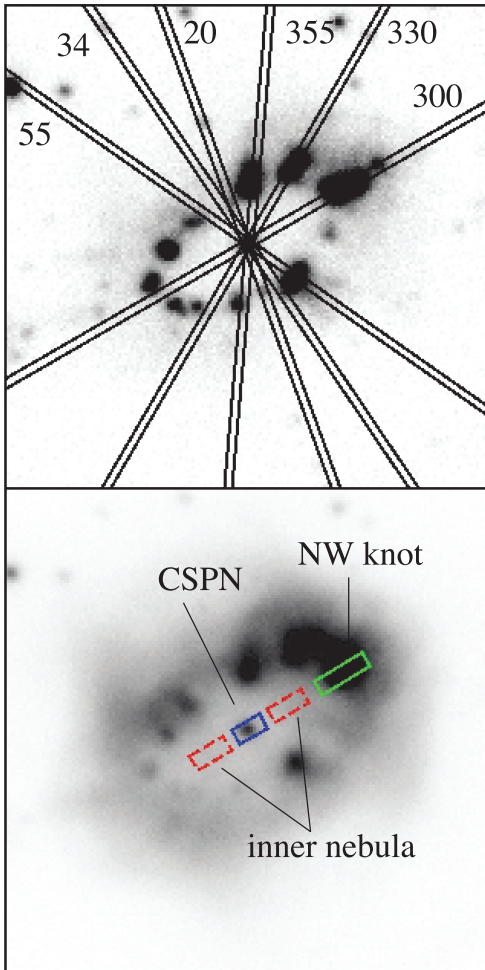


Figure 2. Position of the slits used for spectroscopy at the NOT (top) and at the WHT (bottom) are shown over a 30×30 arcsec² zoom of the [N II] and [O III] images, respectively, with linear intensity scale. In the latter, the central star (CSPN) and the two regions of the nebula discussed in the text are indicated.

Time-resolved photometry in the Sloan Digital Sky Survey (SDSS) i band of IPHASX J194359.5+170901 was performed during 2009 with the 1.2-m Mercator telescope and its MEROPE camera, the 2.5-m Isaac Newton Telescope (INT) and its Wide Field Camera (WFC), and the 0.8-m IAC80 and its CAMELOT camera. The time coverage of each set of images was different, while the individual exposure times were chosen to ensure a signal-to-noise ratio (S/N) ~ 120 on the integrated emission from the central star. In the case of the MERCATOR/MEROPE observations, the time coverage was split into two blocks separated by several hours to better sample variability. The log of the photometric observations can be found in Table 1. Magnitudes obtained with different telescope/filter combinations were matched to the INT SDSS i photometric system using field stars. The data are listed in Table 2.

All data were reduced using standard routines in IRAF.

3 MORPHOLOGY, KINEMATICS, GEOMETRY AND ORIENTATION

The morphology of the nebula (Fig. 1) is similar in the $H\alpha$ and [O III] emission: it consists of a diffuse, elliptical or perhaps spindle-like inner body, whose brightest regions are in the form of a knotty ellip-

Table 1. Log of the photometric observations of IPHASX J194359.5+170901.

Date (2009)	Instrument	Filter	Exp. time (s)	Coverage (min)
Aug 25	MEROPE	Cousins I	200	2×25
Aug 28	MEROPE	Cousins I	200	2×20
Aug 31	MEROPE	Cousins I	200	2×60
Sep 1	MEROPE	Cousins I	200	60+15
Sep 2	MEROPE	Cousins I	200	75
Sep 10	CAMELOT	Johnson I	600	90
Oct 25	WFC	SDSS i	60	180

Table 2. SDSS i magnitudes of the central star of IPHASX J194359.5+170901. A small sample is provided below, the full table being available in the electronic version of the article (see Supporting Information).

HJD	i -mag	Error
245 5069.452 360	17.90	0.02
245 5069.455 140	17.91	0.02
245 5069.457 900	17.89	0.02
245 5069.460 670	17.87	0.02
245 5069.463 420	17.87	0.02
245 5069.466 190	17.86	0.02
245 5069.468 930	17.89	0.02
245 5069.471 730	17.87	0.02
245 5069.535 730	17.69	0.02
245 5069.538 470	17.69	0.02
245 5069.541 210	17.68	0.02
245 5069.543 990	17.70	0.02
245 5069.546 760	17.71	0.02
....		

tical ring with a long axis of about 13 arcsec. Along the orthogonal direction, faint emission traces a roughly cylindrical structure ending in two slightly brighter, irregular ‘polar’ caps at about 1 arcmin from the central star. As typical of this kind of structure (Gonçalves, Corradi & Mampaso 2001), the ring’s knots and their faint outward tails, as well as the polar caps, are most evident in the low-ionization [N II] emission. This striking [N II] morphology led to the object’s nickname, ‘the Necklace nebula’ (Sabin et al. 2010, in preparation).

The kinematics and 3D structure of the nebula were studied by means of the Doppler shift of the [N II] 6583 line (which has a smaller thermal broadening than $H\alpha$) in the NOT spectra. The [N II] line-of-sight velocities at the position of the ring’s knots are well fitted (Fig. 3) by a circular expanding ring with the following parameters: ring radius $r = 6.5 \pm 0.5$ arcsec, inclination to the plane of the sky $i = 59^\circ \pm 3^\circ$ (where $i = 0^\circ$ is the ring in the plane of the sky and $i = 90^\circ$ is in the line of sight), major axis of the ring projected on the sky at $PA = 122^\circ \pm 3^\circ$, expansion velocity $V_{\text{ring}} = 28 \pm 3$ km s⁻¹ and systemic velocity $V_{\text{sys}} = 45 \pm 2$ km s⁻¹, corrected to the local standard of rest. The distance-dependent age of the ring, assuming no acceleration, is $tD_{\text{ring}}^{-1} = 1100$ yr kpc⁻¹.

The [N II] velocities of the polar caps are shown in Fig. 4. Assuming that they are located along the polar axis of the ring, their deprojected mean velocities are 115 km s⁻¹ for the southern cap, and 95 km s⁻¹ for the northern one.

Their age/distance parameter tD_{caps}^{-1} is between 1900 (part of the southern cap closer to the star) and 2800 yr kpc⁻¹ (outermost region of the southern cap). This is roughly twice as large as for the ring.

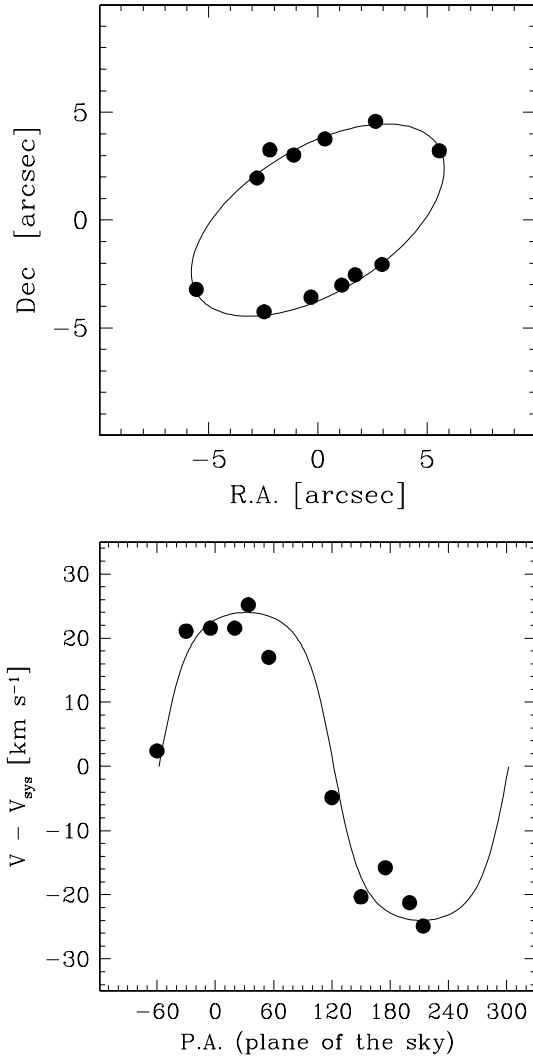


Figure 3. The ring’s kinematical fit. Top: dots indicate the positions at which radial velocities are measured, i.e. the intersection of the NOT slits with the brightest part of the ring. Bottom: dots are the corresponding [N II] line-of-sight velocities. Solid lines show the fit to the data with an inclined, circular expanding ring with the parameters quoted in the text.

Thus, in the simple hypothesis of ballistic motions, the caps must have been ejected before the ring. The lack of a clear increase of speed with distance from the central star *along* each cap might also suggest a continuous ejection process that lasted for a significant length of time, during a now extinct jet phase perhaps.

The limited resolution and depth of the NOT spectra do not allow us to perform a kinematical study of the faint emission extending from the ring to the caps.

We conclude that the morphology of the IPHASX J194359.5+170901 nebula is that of an ‘equatorial’ ring, where most of the emission (ionized mass) is concentrated, from which faint lobes depart, ending in low-ionization ‘polar’ caps.

4 CHEMICAL ABUNDANCES

The WHT spectrum was used to compute the physical and chemical properties of the nebula. Three regions were considered (see Fig. 2, bottom panel): the central star (CSPN), discussed in the next

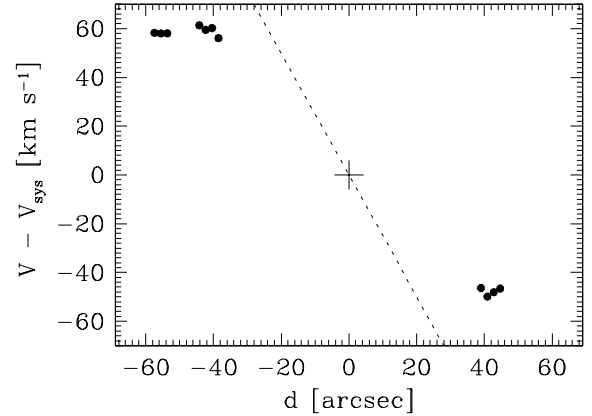


Figure 4. The observed [N II] velocities in the polar caps (dots). The dotted line shows the variation of velocities with distance from the central star, assuming a proportionality law with a slope fixed by the expansion speed of the ring.

section; the *inner nebula* contained within a distance from 1.6 to 4.0 arcsec on both sides of the CSPN and the bright NW knot extending from 5.0 to 8.4 arcsec on the NW side of the CSPN. The emission-line fluxes for the nebular regions are listed in Table 3: the errors quoted include both the uncertainty in the flux of each line (Poissonian, detector and background noise) and the determination of the instrumental sensitivity function for flux calibration.

The logarithmic extinction at $H\beta, c_{\beta}$, was computed from the hydrogen Balmer decrement by averaging the results from the observed $H\alpha/H\beta, H\gamma/H\beta$, and $H\delta/H\beta$ ratios (weighted by their errors) in the two nebular regions. Owing to the high excitation of the nebula, the hydrogen Balmer lines are contaminated by unresolved He II Pickering lines at a level of 6 per cent for the inner nebula and 4 per cent for the knot. This contribution does not significantly affect the calculation of c_{β} , but must be subtracted when the elemental abundances are computed (see below).¹ The extinction law by Fitzpatrick (2004) with $R = 3.1$ was adopted. The theoretical Balmer line ratios were derived from Blocklehurst (1971) for electron temperatures as determined below. We obtained $c_{\beta} = 0.55 \pm 0.06$, corresponding to $A_V = 1.19 \pm 0.12$. Line fluxes dereddened using this c_{β} and the Fitzpatrick’s extinction law are also listed in Table 3.

The nebula of IPHASX J194359.5+170901 is of high excitation. In the inner nebula, after dereddening [O III] 5007 is the strongest line followed by [Ne V] 3426. He II 4686 is stronger than $H\beta$, indicating the highest excitation class (10) according to the scheme set out by Dopita & Meatheringham (1990). In the NW knot, excitation is slightly lower as He II and [Ne V] are relatively weaker, albeit the [O III]/ $H\beta$ ratio is larger than in the inner nebula. This suggests, as confirmed by the chemical analysis below, that most of the oxygen in the inner nebula is in higher ionization stages which are not observed in the optical. This also holds for other elements including nitrogen and sulphur. In the knot, neutral species like [O I] and [N I] are also present. The mixture of high- and low-ionization atoms is only partly caused by the superposition along the line of sight of the high-excitation gas belonging to the main body of the nebula with the relatively lower ionization of the ring’s knots.

The electron densities N_e were computed from the [S II] 6731/6717 line ratio and, in the inner nebula, also from the [Ar IV]

¹ Note that fluxes in Table 3 are the observed ones, and include the contribution of the He II lines to the H I emission.

Table 3. Observed (F_{obs}) and dereddened (F_{der}) nebular emission line fluxes, relative to $H\beta = 100$ and their errors. H Balmer lines include the contribution of He II Pickering lines (see text).

Identification	λ_{obs} (Å)	Inner nebula				NW knot			
		F_{obs}	Error (per cent)	F_{der}	Error (per cent)	F_{obs}	Error (per cent)	F_{der}	Error (per cent)
He II 3203.1	3201.1	25.6	7	46.8	9	18.1	8	33.0	10
[Ne V] 3345.4	3344.3	59.9	4	102.0	7	7.7	10	13.1	12
[Ne V] 3425.5	3424.6	173.8	3	286.4	6	19.6	4	32.2	7
O III 3444.1?	3442.5					3.0	15	5.0	16
[O II] 3726+3729	3726.8	6.0	20	8.9	21	84.4	3	125.0	5
H I 3750.1	3749.6					1.8	24	2.6	24
He I 3756.1blend	3755.8					2.9	18	4.3	19
H I 3770.6	3770.6					2.8	11	4.1	12
H I 3797.9	3797.3	3.7	14	5.3	15	3.5	9	5.1	10
H I 3835.3	3835.0	4.9	9	7.0	10	4.4	7	6.2	8
[Ne III] 3869.0	3868.5	25.0	4	35.4	5	78.3	3	110.7	5
H I 3889.0	3888.8	7.8	7	10.9	8	10.3	5	14.4	6
[Ne III]+He II	3968.0	18.8	5	25.7	6	36.0	3	49.1	5
He II 4025.6	4025.8					1.3	24	1.7	24
[S II] 4068.6	4068.7					4.0	8	5.3	8
[S II] 4076.3	4076.6					1.0	20	1.3	20
H I 4101.7	4101.7	20.1	4	26.2	5	19.9	4	25.9	5
He II 4199.8	4200.5	1.9	25	2.4	25	1.1	25	1.4	25
H I 4340.5	4340.5	39.7	3	47.5	4	38.5	3	46.0	4
[O III] 4363.2	4363.3	7.9	7	9.4	7	13.9	4	16.5	4
He I 4471	4471.8					2.3	11	2.6	11
He II 4541.6	4541.5	3.6	12	4.0	12	2.6	10	2.9	10
He II 4685.7	4685.7	105.2	3	111.6	3	79.6	3	84.4	3
[Ar IV] 4711.4	4711.6	17.1	4	18.0	4	9.3	4	9.8	4
[Ar IV] 4740.2	4740.1	12.6	5	13.1	5	6.9	5	7.1	5
H I 4861.4	4861.2	100.0	3	100.0	3	100.0	3	100.0	3
[O III] 4958.9	4958.8	179.3	3	173.7	3	436.8	3	423.1	3
[O III] 5006.8	5006.7	534.6	3	510.0	3	1280.7	3	1221.6	3
[N I] 5199	5198.6					3.7	9	3.4	9
He II 5411.5	5411.9	9.4	30	7.9	30	7.5	30	6.3	30
[Cl III] 5517.7	5518.0	1.2	33	1.0	33	2.2	15	1.8	15
[Cl III] 5537.9	5538.5	0.7	47	0.6	47	1.8	19	1.5	19
[N II] 5754.64	5754.8					4.2	6	3.2	6
He I 5875.6	5875.7	1.8	29	1.3	29	8.2	6	6.2	6
[O I] 6300.3	6300.1					19.8	3	13.4	5
[S III] 6312.1	6312.1	4.8	7	3.3	8	9.8	4	6.6	6
[O I] 6363.8	6363.7					6.7	4	4.4	6
[Ar V] 6434.7	6435.2	7.2	5	4.7	7	1.1	18	0.7	18
He II 6527.1	6526.6	1.9	20	1.2	20				
[N II] 6548.1	6547.9	5.3	8	3.4	9	93.7	3	60.2	6
H I 6562.8	6562.7	416.8	3	267.1	6	460.0	3	294.8	6
[N II] 6583.4	6583.2	12.7	4	8.1	7	298.1	3	190.2	6
He I+He II	6679.3					3.8	7	2.4	8
He II 6683.2	6682.3	2.1	18	1.3	18				
[S II] 6716.4	6716.3	3.9	8	2.4	10	48.2	3	29.9	6
[S II] 6730.8	6730.6	3.3	11	2.1	12	51.7	3	32.0	6
He II 6890.9	6890.9	1.5	25	0.9	25	1.4	17	0.9	18
[Ar V] 7005.4	7005.9	17.1	4	10.1	7	2.6	10	1.5	11
He I 7065	7064.9					2.6	9	1.5	11
[Ar III] 7135.8	7135.7	23.9	3	13.8	7	57.3	3	33.0	7
[Ar IV]+He II	7175.6					2.1	13	1.2	14
[O II] 7319	7319.1					7.1	5	4.0	8
[O II] 7330	7329.6					5.7	5	3.2	8
[Cl IV] 7530	7529.8	1.6	24	0.9	25	1.7	18	0.9	19
He II 7592.7	7592.3	3.1	24	1.7	25	1.9	36	1.0	37
[Ar III] 7751.1	7750.9	5.6	7	2.9	10	15.0	4	7.9	8
[Cl IV] 8046.3	8045.9	4.9	8	2.5	11	3.2	9	1.6	12
He II 8236.8	8236.9	5.3	7	2.6	10	4.5	7	2.2	11
H I 8545.4	8545.2					1.1	28	0.5	29
H I 8598.4	8598.5	1.6	28	0.8	29	2.1	12	1.0	15

Table 3 – *continued*

Identification	λ_{obs} (Å)	Inner nebula				NW knot			
		F_{obs}	Error (per cent)	F_{der}	Error (per cent)	F_{obs}	Error (per cent)	F_{der}	Error (per cent)
H I 8665.0	8664.6	1.2	21	0.6	23	2.4	10	1.1	13
H I 8750.5	8750.2	2.3	22	1.1	24	2.4	13	1.1	15
H I 8862.8	8862.1					3.4	13	1.6	15
H I 9014.9	9014.3	3.6	15	1.6	17	4.0	9	1.8	12
[S III] 9068.6	9068.8	46.3	3	20.9	9	109.4	3	49.4	9

4711/4740 ratio. The electron temperature T_e was computed from the [O III] (5007+4959)/4363 ratio and, in the NW knot, also the [N II] (6583+6548)/5755 ratio. The NEBULAR package in IRAF (Shaw & Dufour 1995) was used, and results are listed in Table 4. Other indicators of density ([Cl III] 5518/5538) and temperature ([O II] (3726+3729)/(7320+7330), [S II] (6717+6731)/4072, [S III] (9069+9532)/6312) are available in the spectra, but the associated errors (from both the line measurements and the uncertainty on temperature/density) are much larger than for the adopted diagnostic ratios, and were therefore not used. The [N II] T_e in the knot is 2000 K lower than the [O III] T_e : this is typical of high-excitation PNe (Kingsburg & Barlow 1994; Perinotto & Corradi 1998), as is the quite large value of T_e in the inner nebula. Densities in IPHASX J194359.5+170901 are conversely relatively low.

Given the temperatures and densities, the ionic abundances relative to hydrogen for all elements but helium were computed from the line fluxes relative to H β using the IONIC task in IRAF. Before the ionic abundances are computed, the contribution of the He II 8–4 Pickering line has been subtracted from the H β line.

For the knot's spectrum, we have adopted the observed [O III] T_e for medium- and high-excitation species (doubly ionized metals or in higher ionization stages), and the [N II] T_e for the lower ionization species. For the inner nebula, the [N II] T_e is not determined directly, and a value of $11\,000 \pm 2000$ K was adopted. This is similar to the electron temperature in the knot's spectrum, fits the empirical relationship between T_e ([N II]) and T_e ([O III]) and the He II 4686 line intensity of equation (2) in Kingsburg & Barlow (1994), and is slightly larger than predicted by equation (3) of Kingsburg & Barlow (1994) and by Magrini et al. (2003). The concentration of helium ions relative to hydrogen was derived from the usual recombination lines assuming case B with the effective recombination coefficients from Hummer & Storey (1987) for the He II and H β lines, and from Benjamin, Skillman & Smits (1999) for the He I lines.

Errors were derived by propagating both the errors in the line measurement and those on the adopted temperature and density. When the ionic abundance of an element is estimated from several independent emission lines, the weighted mean and its standard deviation were computed. To obtain the total abundances, we used the ionization correction factors (*icfs*) listed in Alexander & Balick (1997), whose primary source is Kingsburg & Barlow (1994). For chlorine, we adopt the *icf* formulation by Kwitter & Henry (2001). Errors on the total abundances are obtained by propagating the errors on the mean ionic abundances as well as on the *icfs*. Ionic and total abundances, and their errors, are listed in Table 4. Note that the total abundances in the inner nebula are not quoted for any element except helium. This is because most of the gas is in high-ionization stages which are not measured, making the *icfs* (120 for nitrogen!) and their errors, and thus the computed abundances, very large. The problem is less severe in the lower ionization NW knot.

Table 4. Physical conditions and chemical abundances in the IPHASX J194359.5+170901 nebula. Total abundances of most metals in the inner nebula are not quoted, given their large *icfs* (see text).

	Inner nebula	NW knot
[S II] N_e	360^{+380}_{-240} cm $^{-3}$	820^{+140}_{-120} cm $^{-3}$
[Ar IV] N_e	370^{+800}_{-370} cm $^{-3}$	
[O III] T_e	14800^{+530}_{-460} K	12960^{+460}_{-400} K
[N II] T_e	$[11000^{+2000}_{-2000}$ K] a	10920^{+420}_{-380} K
He $^+$ /H $^+$	0.011 ± 0.003	0.052 ± 0.005
He $^{2+}$ /H $^+$	0.105 ± 0.016	0.077 ± 0.009
He/H	0.116 ± 0.016 (11.06) b	0.129 ± 0.010 (11.11) b
O $^+$ /H $^+$ $\times 10^4$	$0.025^{+0.044}_{-0.014}$	0.43 ± 0.13
O $^{2+}$ /H $^+$ $\times 10^4$	0.59 ± 0.06	2.00 ± 0.20
<i>icf</i> (O)		1.83 ± 0.15
O/H $\times 10^4$		4.45 ± 0.57 (8.64) b
N $^+$ /H $^+$ $\times 10^4$	$0.015^{+0.009}_{-0.004}$	0.30 ± 0.03
<i>icf</i> (N)		10.36 ± 3.40
N/H $\times 10^4$		3.11 ± 1.07 (8.49) b
log (N $^+$ /O $^+$)	-0.23 ± 0.60	-0.15 ± 0.20
Ne $^{2+}$ /H $^+$ $\times 10^4$	0.098 ± 0.015	0.45 ± 0.08
Ne $^{4+}$ /H $^+$ $\times 10^4$	0.71 ± 0.10	0.13 ± 0.02
<i>icf</i> (Ne) c		2.23 ± 0.36
Ne/H $\times 10^{4c}$		1.00 ± 0.24 (8.00) b
Ne/H $\times 10^{4d}$	1.21 ± 0.15 (8.08) b	0.87 ± 0.12 (7.94) b
Ar $^{2+}$ /H $^+$ $\times 10^6$	0.57 ± 0.06	1.81 ± 0.19
Ar $^{3+}$ /H $^+$ $\times 10^6$	1.10 ± 0.10	0.79 ± 0.07
Ar $^{4+}$ /H $^+$ $\times 10^6$	0.94 ± 0.10	0.18 ± 0.03
<i>icf</i> (Ar)		1.11 ± 0.04
Ar/H $\times 10^6$		3.08 ± 0.26 (6.49) b
S $^+$ /H $^+$ $\times 10^6$	0.093 ± 0.036	1.29 ± 0.21
S $^{2+}$ /H $^+$ $\times 10^6$	2.33 ± 0.45	7.02 ± 1.40
<i>icf</i> (S)		1.56 ± 0.46
S/H $\times 10^6$		13.98 ± 4.43 (7.15) b
Cl $^{2+}$ /H $^+$ $\times 10^7$	0.37 ± 0.12	1.07 ± 0.19
Cl $^{3+}$ /H $^+$ $\times 10^7$	1.01 ± 0.20	0.80 ± 0.49
<i>icf</i> (Cl)		2.48 ± 0.31
Cl/H $\times 10^7$		4.64 ± 1.42 (5.67) b

a Adopted (see text).

b Total abundances expressed as $\log(X/H) + 12$.

c Ne/H = *icf* \times (Ne $^{2+}$ /H $^+$) (Kingsburg & Barlow 1994).

d Ne/H = $1.5 \times$ (Ne $^{2+}$ /H $^+$ + Ne $^{4+}$ /H $^+$) (Kingsburg & Barlow 1994).

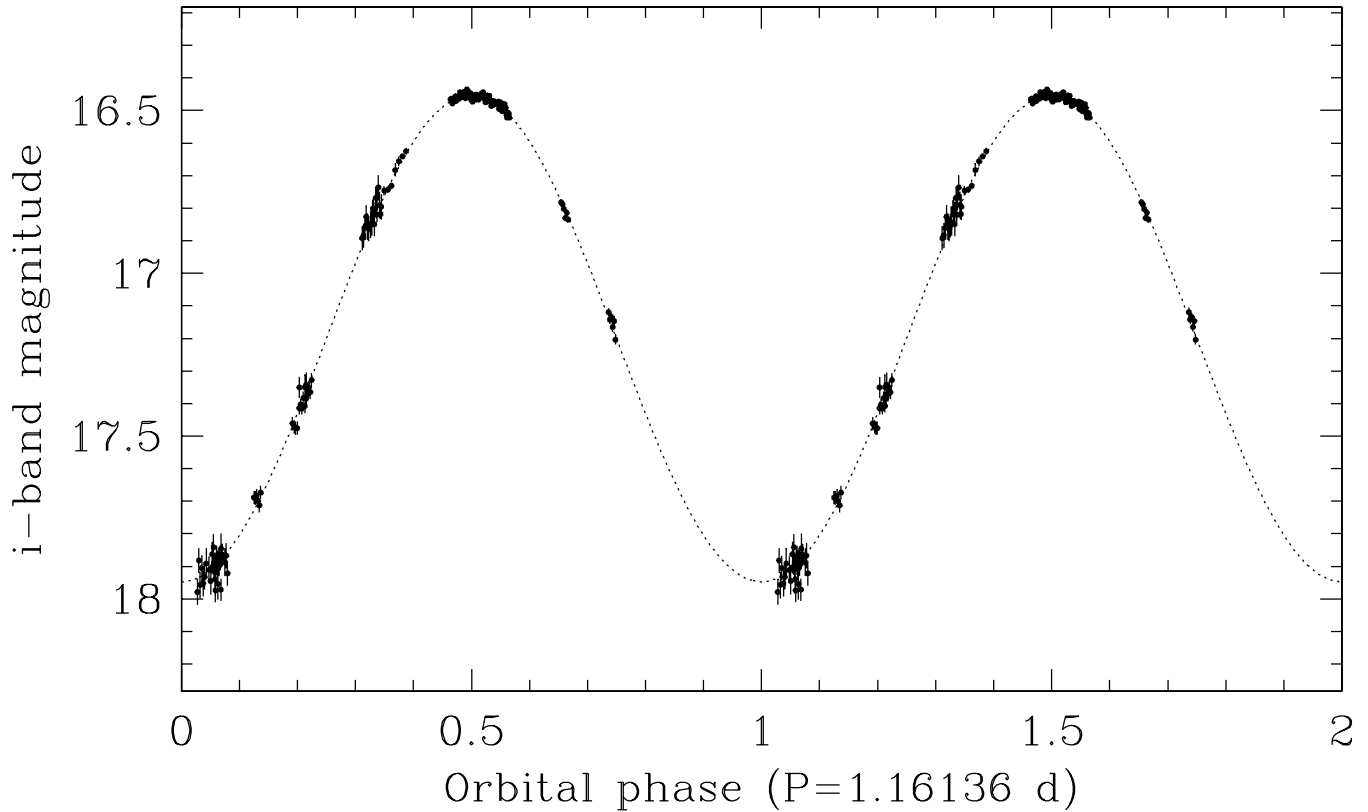


Figure 5. The folded light curve of the IPHASX J194359.5+170901 central star.

According to the chemical abundances computed in the ring’s knot, IPHASXJ194359.5+170901 is located just on the side of type I PNe in the He/H versus N/O diagram, within the range covered by bipolar PNe (Perinotto & Corradi 1998). However, the N/O and He/H overabundances are mild and their errors are non-negligible. Abundances for the other elements are typical of the majority of PNe (cf. table 3 in Perinotto & Corradi 1998 and table 14 in Kingsburg & Barlow 1994).

5 THE BINARY CENTRAL STAR

5.1 Light curve

The central star’s coordinates are RA=19^h43^m59^s.51 and Dec.=+17°09′00″.9 (J2000). Its light curve in the *i* band from data in Table 2, folded on the period determined below, is shown in Fig. 5.

The photometric data set was subjected to a period analysis using Schwarzenberg-Czerny’s (Schwarzenberg-Czerny 1996) analysis-of-variance (AOV) method implemented in MIDAS. The AOV periodogram shows the strongest peak at ~ 0.86 cycle d^{-1} , which corresponds to a period of 1.16 d. A sine fit to the whole data set results in $P = 1.16136 \pm 0.00002$ d, an *i*-band amplitude (defined as half the peak-to-peak variation) of 0.747 ± 0.002 mag (among the largest known in this class of objects) and an average magnitude of 17.199 ± 0.002 mag. The fit is shown as a dotted line in Fig. 5. Uncertainties quoted above are the formal errors of the fit: a better sampling of the curve at all phases is needed to refine the period and fix the error. In any case, we take the observed CSPN variability as a clear indication of binarity, the brightness modulation being the result of observing the irradiated side of a companion, heated by the hot core that ejected the PN, at different angles during

the orbital motion. This is supported by the spectrum presented in next section. Within this hypothesis, maximum brightness occurs at $245\,5075.7780 \pm 0.0007$ (HJD), at orbital phase $\Phi = 0.5$ i.e. at inferior conjunction of the hot component.

The amplitude of reflection effect seen here is at the high end, but compatible with those seen in a range of young post-common envelope (CE) binaries (Aungwerojwit et al. 2007).

5.2 The irradiated spectrum

The spectrum of the CSPN is shown in Fig. 6. It consists of a continuum slowly declining with increasing wavelength and a rich set of emission lines. In the figure, the contribution from the extended nebula was subtracted by interpolating nebular regions on the opposite sides of the CSPN and as close to it as possible. The subtraction is generally accurate, except at the wavelengths of the brightest nebular lines (mainly He II 4686, H β and H α). At the resolution (3 Å) and S/N ratio (~ 25) of the blue side of our spectrum, no absorption lines from the hot ionizing CSPN are detected (the feature at He II 4686 is likely a nebula subtraction residual). The phase of the orbital period for this spectrum is not known, as the period parameters are not precise enough to trace it back to 2007.

As in similar close binary CSPNs (e.g. BE UMa, $P = 2.3$ d; Ferguson & James 1994), the high order lines of the H I Balmer and (fainter) Paschen sequences are observed in emission. The Balmer decrement, which has a better S/N ratio and resolution, is remarkably flat from H γ to the highest order transitions. Information for H β and H α is limited by the uncertainty in the subtraction of the overlapping nebula, as mentioned above, but the two lines are definitely weaker than H δ . In BE UMa, this flat Balmer decrement is explained as an optical depth effect in the dense irradiated atmo-

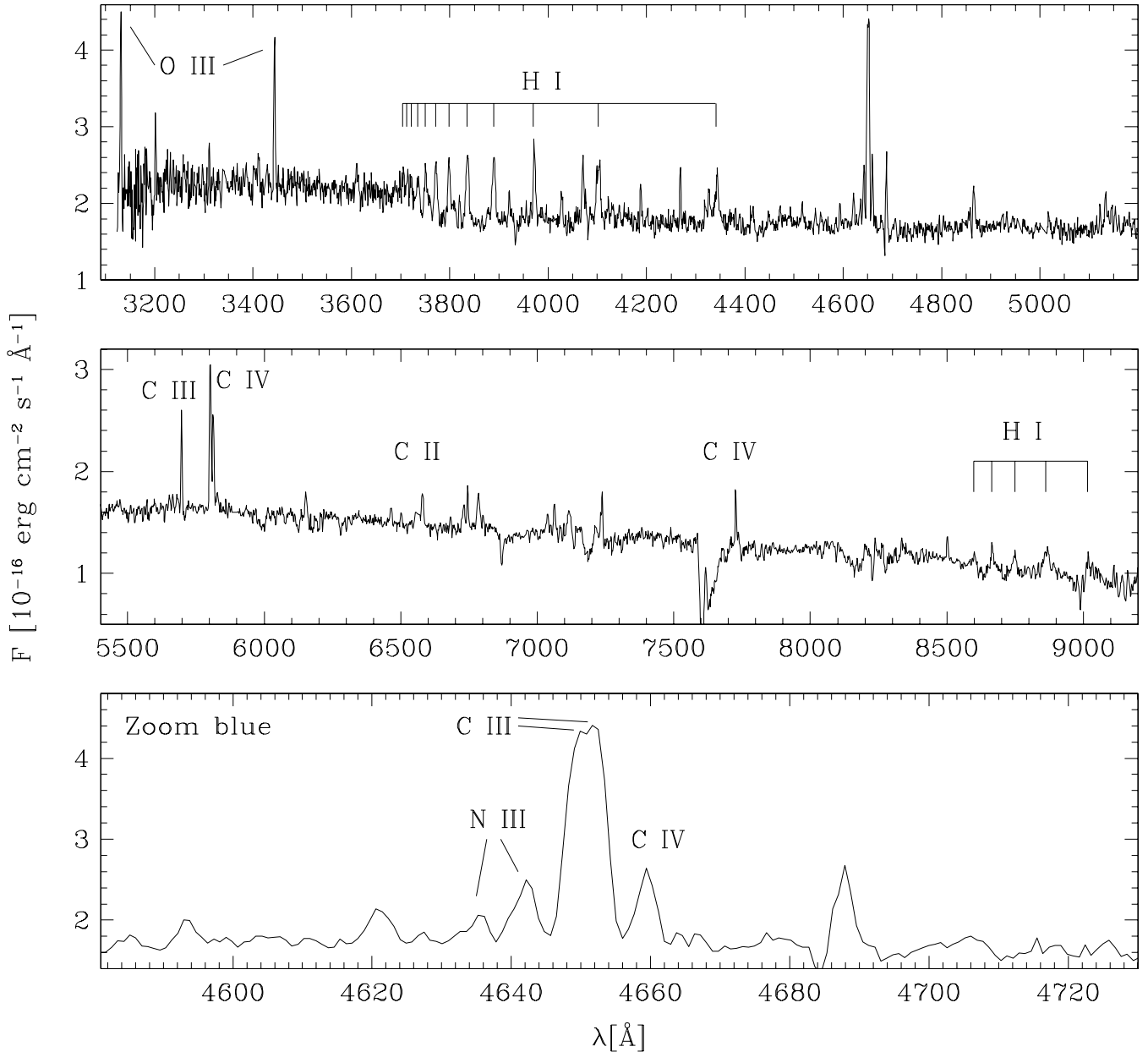


Figure 6. The blue (top) and red (middle) parts of the WHT spectrum of the central star of IPHASX J194359.5+170901. At the bottom, a zoom of the blue side of the spectrum around the blend at 4650 \AA is displayed.

sphere of the secondary (Ferguson & James 1994). The high-order Balmer lines are resolved (FWHM $\sim 5 \text{ \AA}$, after correcting for the instrumental width) which can be explained by Stark broadening. As in BE UMa, the Balmer jump is seen in emission.

The spectrum shows a number of narrow (unresolved) emission lines, which are also assumed to come from the irradiated side of the secondary. The most prominent group is the blend around 4650 \AA (bottom panel of Fig. 6). Given the presence of strong O III lines at 3131 and 3444 \AA , the origin of some lines of this blend may be explained by the Bowen fluorescence mechanism (Bowen 1934), which would result in the formation of the N III lines observed at 4635 and 4641 \AA . The peak of the blend is resolved in two components which are identified as the 3S–3P_o C III transitions at 4649 and 4652 \AA . This is preferred to the alternative identification of lower excitation O II lines (but a contribution of both is not excluded), because of a better wavelength match, and because

the C III 5696, C IV 4658, C IV 5801 and C IV 5812 lines are also observed, showing a quite high degree of excitation in the irradiated spectrum of IPHASX J194359.5+170901. This is higher than in e.g. BE UMa, where no C IV lines are detected, but similar to e.g. V477 Lyrae (Pollacco & Bell 1994) and ETHOS1, another new PN with a close binary nucleus (Miszalski et al. in preparation). Other C III and C II lines, as well as low- and high-excitation narrow lines of other elements, are tentatively identified in the WHT spectrum of IPHASX J194359.5+170901. Given the limited spectral resolution, and the uncertainty in the Doppler shift (and hence of the line identification) introduced by the unknown contribution of the orbital motion, we defer a more detailed analysis of the emission line spectrum when higher quality data and a radial velocity curve are obtained.

The continuum, dereddened using $A_V = 1.19$ (Section 4), cannot be fit by a single blackbody over the whole observed spectral range

(3200–9200 Å). A single blackbody with $T = 8000$ K provides a reasonably good fit only for $\lambda > 5000$ Å, while a good fit to the whole spectral range is obtained with a blackbody temperature between 6000 and 7000 K (typical of an F-type star) plus an additional much hotter component – presumably the ionizing/irradiating primary – whose contribution would dominate the emission at wavelengths shorter than 4000–5000 Å. The temperature estimated for the re-processed component of the secondary atmosphere is similar to that determined for the companion in BE UMa.

6 DISTANCE, MASS, SIZE AND AGE

The distance to IPHASX J194359.5+170901 can be estimated using the relation between the $H\alpha$ surface brightness and radius of the nebula (Frew & Parker 2006). This can be seen as a variant of the mass–radius relationship (e.g. Daub 1982), but it has been carefully calibrated over a large range of sizes and surface brightnesses and for different classes of PNe. The radius of IPHASX J194359.5+170901, computed as the geometric mean of the major and minor semi-axes of the inner elliptical body of the nebula defined at 10 per cent peak brightness, is $r = 10.5$ arcsec. The dereddened mean surface brightness of the nebula within this ellipse is $S(H\alpha) = 6.1 \pm 1.3 \times 10^{-15}$ erg cm⁻² s⁻¹ arcsec⁻². It was computed by combining the flux-calibrated $H\alpha$ + $[N\ II]$ IPHAS images, the narrow-band NOT images which separate the $[N\ II]6583$ and $H\alpha$ emission, and the flux-calibrated WHT spectra. These figures, included in the updated log–log correlation between radius and surface brightness for the subsample of high-excitation, optically thin PNe² like IPHASX J194359.5+170901, result in a distance $D = 4.6 \pm 1.1$ kpc. The quoted error includes the measured uncertainties on $S(H\alpha)$, combined in quadrature with the dispersion in the correlation (Frew 2008).

IPHASX J194359.5+170901 is located close to the Galactic plane ($b = -3.37^\circ$) at longitude $l = 54^\circ 16'$. The systemic velocity of the nebular ring ($V_{LSR} = +45$ km s⁻¹; see Section 3), assuming that the nebula participates in the general circular rotation around the Galactic Centre, would imply a lower limit of 1.6 kpc for the distance, at 1σ of the estimated error which is mainly due to the velocity dispersion ellipsoids of stars in the Galaxy (Nordström et al. 2004).

For a distance of 4.6 kpc, the ionized mass of its nebula computed from the total $H\alpha$ flux and for a standard choice of the filling factor (0.4, with a 100 per cent uncertainty due to the highly aspherical geometry of the nebula) is $0.06 \pm 0.03 M_\odot$, within the range of masses determined for other PNe (Frew & Parker 2010). The total size of the nebula, including the faint polar extensions, is considerable, 2.7 pc. The kinematical age of the ring would be 5000 yr, and the maximum age of the polar caps would be 13 000 yr.

7 DISCUSSION

IPHASX J194359.5+170901 is a new Galactic PN with remarkable properties. Its IAU-approved name is PN G054.2-03.4. Analysis of the images and the $[N\ II]$ line Doppler shifts indicate that its symmetry axis is inclined to the line of sight by 59° , that most of the gas was ejected in an ‘equatorial’ direction corresponding to the observed knotty ring, and that faint ‘polar’ extensions culminate in

low-ionization caps travelling at a speed of roughly 100 km s⁻¹. The kinematical data would suggest a sequence of ejection from the progenitor consisting of a (continuous?) polar outflow during several 10^3 yr, followed, a few 10^3 yr later, by the ejection of the envelope along the equatorial direction. A similar age difference between the high-velocity polar outflow and the inner nebula is computed for Abell 63 (Mitchell et al. 2007) and Hb 12 (Vaytet et al. 2009) which have a confirmed or suspected binary CSPN, respectively. This picture is however based on the simplistic assumption of ballistic motion, and does not take into account acceleration/deceleration due to the hydrodynamical evolution of the structures, as well as possible slowing down of gas with time by interaction with the environment, which would reduce the age difference with respect to the main equatorial outflow. Note also that this result apparently contradicts the finding that in proto-PNe jets are produced slightly later than equatorial tori (Huggins 2007). These molecular tori expand at a lower speed than the ionized ring of IPHASX J194359.5+170901, which might indicate different ejection processes or a significant acceleration of the gas after photoionization and the fast wind from the central star arise. However, the two samples do not seem to be evolutionary linked as no evidence for close binary central stars are found in the proto-PN objects (Hrivnak 2010, in preparation).

The main result of this study is the discovery that the central star of IPHASX J194359.5+170901 is a close binary. Its orbital period is 1.16 d. This lies at the longer tail of the binary CSPN period distribution (Miszalski et al. 2009a), and implies that the system went through CE evolution before the ejection of the PN, which made the orbit shrink to the present value. The recent discovery of a significant number of PN binary central stars (Miszalski et al. 2009a), provides the base for a better understanding of the effects of binarity on the mass-loss processes at the end of stellar evolution. IPHASX J194359.5+170901 supports the increasing evidence in PNe (but not in proto-PNe, see above) of a correlation between the appearance of morphological features like rings and collimated high-velocity outflows with the presence of a close binary central star (Miszalski et al. 2009b). Strictly speaking, Abell 63 (Mitchell et al. 2007) and IPHASX J194359.5+170901 are the only PNe with a close binary central star for which the presence of a high-velocity collimated outflow along the symmetry axis of the main nebula (i.e. the polar directions) has been demonstrated. In NGC 6337, a supersonic collimated outflow is also detected, but its orientation with respect to the main nebular ring is not completely clear (Corradi et al. 2000; García-Díaz et al. 2009). Other close binary PNe with similar polar outflows are likely to be Sab 41 (Miszalski et al. 2009b) and ETHOS1 (Miszalski et al. 2010), but kinematical data are needed to confirm this. Most of the other cases quoted in the literature (see De Marco 2009), like the well studied object, K 1–2, are instead dubious identifications (Corradi et al. 1999; Miszalski et al. 2009b), mainly because of the lack of convincing evidence for large expansion speeds.

Another notable characteristic of IPHASX J194359.5+170901 is its prominent equatorial ring, a morphological feature that appears to be distinctive of PNe with close binary central stars (Miszalski et al. 2009b). Clear examples are the already cited NGC 6337 and Sab 41, as well as Hen 2–428 (Santander-García et al., in preparation). SuWt 2 also falls in this morphological class, but the nature of the central system (binary or triple?) is less clear (Jones et al. 2010). Note that these marked equatorial outflows are also observed in much wider binaries like the symbiotic Miras (e.g. Hen 2-147; Santander-García et al. 2007), as well as in massive stars (Smith, Bally & Walawender 2007) including SN1987A (Plait et al. 1995).

² Note that this subsample includes a number of PNe with close binary CSPNs (Frew & Parker 2007).

Models predict that a sudden envelope ejection results from CE evolution and that it is strongly concentrated towards the orbital plane (Sandquist et al. 1998). This would correspond to the ‘equatorial’ rings/tori observed in a number of these PNe. As discussed for NGC 6337 (Corradi et al. 2000), the clumpy appearance of the ring of IPHASX J194359.5+170901, in the form of low-ionization knots with outward-facing radial tails, can be explained as density fluctuations created during the envelope ejection and later exacerbated by the action of the expanding ionization front or the post-asymptotic giant branch (AGB) fast wind. Alternatively, the ring’s knots would be created by radiative shocks leading to the fragmentation of the shell without involving previous density inhomogeneities. The polar outflow could then be the result of inertial confinement of the gas, forced by the flattened deposition of the envelope, when further shaping of the PN takes place under the action of a fast wind from the post-AGB primary (Icke et al. 1992). Additionally/alternatively, a strong magnetic field in the AGB envelope, especially if spun up by the gain of orbital angular momentum during the CE phase, might play a role in the shaping outflow both in the equatorial plane and in the polar directions (Nordhaus, Blackman & Frank 2007; but see Soker & Harpaz 1992). In such cases, the polar outflow would be produced together with the ring (or later), and therefore the apparent difference in their kinematical ages in IPHASX J194359.5+170901 (and Abell 63 and Hb 12) would not reflect a real age difference.

Another possibility is that the high-velocity polar outflow is produced *before* the CE phase from an accretion disc around the secondary, which can accrete matter from the wind of the primary or via Roche lobe overflow (Soker 1998; Soker & Rappaport 2000). This would explain why the polar outflow has a kinematical age larger than that of the ring.

In all models the above, the inclination of the orbit of the IPHASX J194359.5+170901 CSPN would be the same as of the nebular ring, namely 59° .

The radiation from the hot CSPN causes strong irradiation effects in the illuminated side of the secondary. They dominate the spectrum presented in this paper, and consist of narrow lines of metals with ionization potential as high as 64.5 eV (C IV), relatively broad H I emission in a flat Balmer sequence, and a continuum in the visible range that is fitted by a blackbody with temperature around 6000–7000 K plus a much hotter component. It is clear that these remarkable characteristics invite a more detailed study of the central source, aimed at detecting the spectral signature of the hot ionizing star, determining the radial velocity curve for both components, and modelling the irradiation spectrum to derive the main parameters of the two stars. This is considered the first priority for the future.

With the data presently available, a robust upper limit of $1.0 M_\odot$ for the mass of the secondary can be estimated by converting the apparent magnitude in the *i* band of the CSPN at minimum (corrected for the adopted interstellar reddening and adopting a distance of 4.6 kpc), to an upper limit to the absolute magnitude of the non-irradiated side of the secondary. Assuming a mass between 0.5 and $1.0 M_\odot$ for the hot post-AGB star, the observed photometric period of 1.16 d implies the separation of the two stars to be between 4 and 6 solar radii. In no case, the secondary fills its Roche lobe if it is a main-sequence star, and no mass transfer to the post-AGB star presently occurs in the system.

ACKNOWLEDGMENTS

Based on observations obtained with the 4.2-m WHT and the 2.5-m INT telescopes of the Isaac Newton Group of Telescopes, the 2.6-m

Nordic Optical Telescope operated by NOTSA, the 1.2-m Mercator Telescope operated by the Flemish Community and the 0.8-m IAC80 telescope, operating on the islands of La Palma and Tenerife at the Spanish Observatories of the Roque de Los Muchachos and Teide of the Instituto de Astrofísica de Canarias. The WHT data were obtained as part of the International Time Programme awarded to the IPHAS collaboration.

The work of RLMC, LS, MSG, AM and KV has been supported by the Spanish Ministry of Science and Innovation (MICINN) under the grant AYA2007-66804. We are grateful to Orsola De Marco and Noam Soker for fruitful discussion.

REFERENCES

- Alexander J., Balick B., 1997, *AJ*, 114, 713
 Aungwerojwit A., Gnsicke B. T., Rodriguez-Gil P., Hagen H.-J., Giannakis O., Papadimitriou C., Allende Prieto C., Engels D., 2007, *A&A*, 469, 207
 Benjamin R. A., Skillman E. D., Smits D. P., 1999, *ApJ*, 514, 307
 Bowen I. S., 1934, *PASP*, 46, 146
 Brocklehurst M., 1971, *MNRAS*, 153, 471
 Corradi R. L. M., Perinotto M., Villaver E., Mampaso A., Gonçalves D. R., 1999, *ApJ*, 523, 821
 Corradi R. L. M., Gonçalves D. R., Villaver E., Mampaso A., Perinotto M., Schwarz H. E., Zanin C., 2000, *ApJ*, 535, 823
 Daub C. T., 1982, *ApJ*, 260, 612
 De Marco O., 2009, *PASP*, 121, 316
 Dopita M. A., Meatheringham S. J., 1990, *ApJ*, 357, 140
 Drew J. et al., 2005, *MNRAS*, 362, 753
 Ferguson D. H., James T. A., 1994, *ApJS*, 94, 723
 Fitzpatrick E. L., 2004, in Witt A. N., Clayton G. C., Draine B. T., eds, *ASP Conf. Ser. Vol. 309, Astrophysics of Dust*. Astron. Soc. Pac., San Francisco, p. 33
 Frew D. J., 2008, PhD thesis, Macquarie University, Sydney, Australia
 Frew D. J., Parker Q. A., 2006, in Barlow M. J., Mendez R. H., eds, *IAU Symp. 234, Planetary Nebulae in our Galaxy and Beyond*. Cambridge Univ. Press, Cambridge, p. 49
 Frew D. J., Parker Q. A., 2007, in Corradi R. L. M., Manchado A., Soker N., eds, *Asymmetrical Planetary Nebulae IV*. IAC Electron. Publ., Tenerife, p. 475
 Frew D. J., Parker Q. A., 2010, *Publ. Astron. Soc. Australia*, 27, 129
 García-Díaz Ma.T., Clark D. M., López J. A., Steffen W., Richer M. G., 2009, *ApJ*, 699, 1633
 Gonçalves D. R., Corradi R. L. M., Mampaso A., 2001, *ApJ*, 547, 302
 Huggins P. J., 2007, *ApJ*, 663, 342
 Hummer D. G., Storey P. J., 1987, *MNRAS*, 224, 801
 Icke V., Mellema G., Balick B., Eulderink F., Frank A., 1992, *Nat*, 355, 524
 Jones D., Lloyd M., Mitchell D. L., Pollacco D. L., O’Brien T. J., Vaytet N. M. H., 2010, *MNRAS*, 401, 405
 Kingsburgh R. L., Barlow M. J., 1994, *MNRAS*, 271, 257
 Kwitter K. B., Henry R. B. C., 2001, *ApJ*, 562, 804
 Magrini L., Perinotto M., Corradi R. L. M., Mampaso A., 2003, *A&A*, 400, 511
 Miszalski B., Acker A., Moffat A. F. J., Parker Q. A., Udalski A., 2009a, *A&A*, 496, 813
 Miszalski B., Acker A., Parker Q. A., Moffat A. F. J., 2009b, *A&A*, 505, 249
 Mitchell D. L., Pollacco D., O’Brien T. J., Bryce M., López J. A., Meaburn J., Vaytet N. M. H., 2007, *MNRAS*, 374, 1404
 Nordhaus J., Blackman E. G., Frank A., 2007, *MNRAS*, 376, 599
 Nordström B., Mayor M., Andersen J., 2004, *A&A*, 418, 989
 Oke T. R., 1990, *AJ*, 99, 1621
 Perinotto M., Corradi R. L. M., 1998, *A&A*, 332, 721

- Plait P. C., Lundqvist P., Chevalier R. A., Kirshner R. P., 1995, *ApJ*, 439, 370
- Pollacco D. L., Bell S. A., 1994, *MNRAS*, 267, 452
- Sandquist E. L., Taam R. E., Chen X., Bodenheimer P., Burkert A., 1998, *ApJ*, 500, 909
- Santander-García M., Corradi R. L. M., Whitelock P. A., Munari U., Mampaso A., Marang F., Boffi F., Livio M., 2007, *A&A*, 465, 481
- Schwarzenberg-Czerny A., 1996, *ApJ*, 460, L107
- Shaw R. A., Dufour R. J., 1995, *PASP*, 107, 896
- Smith N., Bally J., Walawender J., 2007, *ApJ*, 134, 846
- Soker N., 1998, *ApJ* 496, 833
- Soker N., Harpaz A., 1992, *PASP*, 104, 923
- Soker N., Rappaport S., 2000, *ApJ* 538, 241
- Vaytet N. M. H., Rushton A. P., Lloyd M., López J. A., Meaburn J., O'Brien T. J., Mitchell D. L., Pollacco D., 2009, *MNRAS*, 398, 385
- Viironen K. et al., 2009, *A&A*, 504, 291

SUPPORTING INFORMATION

Additional Supporting Information may be found in the online version of this article:

Table 2. SDSS *i* magnitudes of the central star of IPHASX J194359.5+170901.

Please note: Wiley-Blackwell are not responsible for the content or functionality of any supporting materials supplied by the authors. Any queries (other than missing material) should be directed to the corresponding author for the article.

This paper has been typeset from a $\text{\TeX}/\text{\LaTeX}$ file prepared by the author.